POLITECNICO
MILANO 1863

SCUOLA DI INGEGNERIA INDUSTRIALE
E DELL'INFORMAZIONE

Simulation of a LEO orbiting microsat on Simulink

MSc in Space Engineering

Authors:

10723712	**Marcello Pareschi**	**(BSc Aerospace Engineering - Politecnico di Milano)**
10836125	**Daniele Paternoster**	**(BSc Aerospace Engineering - Politecnico di Milano)**
10711624	**Alex Cristian Turcu**	**(BSc Aerospace Engineering - Politecnico di Milano)**
10884250	**Tamim Harun Or**	**(BCs)**

Professor: Franco Bernelli Zazzera

Academic year: 2023-2024

Abstract

La presente relazione di prova finale intende dare una descrizione dell'endoreattore F-1 prodotto da Rocketdyne. Cinque di questi motori vennero installati sul primo stadio S-IC del vettore Saturn V che portò il primo uomo sulla luna. L'obiettivo di questo stadio era quello di portare il razzo ad una quota di 61 km, fornendo un $\Delta v \simeq 2300$ m/s. Questo primo requisito verrà mostrato attraverso un modello matematico che simula il volo dello stadio S-IC.
Di seguito verranno analizzati i principali sistemi per un singolo motore, partendo dal sistema di storaggio e alimentazione dei propellenti costituito dai serbatoi e dalla turbopompa, passando per il sistema di generazione di potenza che comprende il gas generator e la turbina. Passando dalla camera di combustione si arriva infine al sistema di espansione gasdinamico e allo studio del suo raffreddamento. Si provvederà inoltre a dare una descrizione qualitativa e quantitativa delle scelte progettuali applicate ai tempi.
La discussione dei processi di combustione del gas generator e della camera di spinta si basa su dati provenienti da simulazioni eseguite con i programmi CEAM e RPA.

Contents

1. Symbols

1.1. Analisi della missione

A_e	$[m^2]$	area di efflusso totale
ϕ	$[rad]$	angolo di traiettoria del razzo

1.2. Analisi della missione 2

A_e	$[m^2]$	area di efflusso totale
ϕ	$[rad]$	angolo di traiettoria del razzo

2. Requirements

2.1. Mandatory requests for simulation

[1]

3. Framework Analysis

3.1. Satellite characterization

3.2. Orbit characterization

4. Dynamics

The equations of the dynamics rotating body motion used throughout the simulation are the Euler equations since rigid body motion assumption is made. The set of equations are referred to the principal axis frame of the satellite. This frame will be also called reference frame $\mathcal{B}$, it is described by three unit vectors $\{\boldsymbol{x_b}, \boldsymbol{y_b}, \boldsymbol{z_b},\}$, that are in the direction of principal inertia axis.

$$\boldsymbol{I}\dot{\boldsymbol{\omega}} + \boldsymbol{\omega} \times \boldsymbol{I}\boldsymbol{\omega} = \boldsymbol{M_d} + \boldsymbol{M_c} \tag{1}$$

In the above equation the external torque has been divided in to 2 contributions, with clear distinction. M_d describes the disturbance torques that act on the spacecraft due to environment and presented in the previous section, while M_c is referred to the control torque that the actuators are generating to perform the tasks required by the control logic.
With particular reference to the Simulink model, two configurations of the satellite were considered: undeployed configuration (for detumbling phase) and extended configuration (for slew and pointing phases). As a consequence, the mass distribution and hence the inertia matrix are different in terms of numerical values. This fact has been taken into account by implementing a logic in the dynamic block of Simulink, that switches between the two matrices using a flag based on the activation of the De-Tumbling control. This istantaneous switch is not completely realistic since the extraction of the panels would require some finite time, and in some way could influence the real dynamic of the satellite. Anyhow, for the microsat considered, the retracted configuration allows a faster detumbling, and also inertia loads and stresses are reduced on the solar panels.

5. Kinematics

As specified in section 2, the attitude parameters of the satellite are expressed through the use of Euler angles. The kinematics calculated according to this parameterization follows these steps:

- given the angular velocity ω from dynamics for each time and the initial condition on Euler angles s_0, compute the time derivatives of the angles $\dot{s}$;
- integrate the derivatives to obtain the set of Euler angles s for each time;
- from the calculated angles, compute the attitude matrix A.

When dealing with this type of parameterization, a major issue arises due to the singularity conditions on the second angle θ for any chosen set of three Euler angles. This can cause the derivatives of the other two angles to tend towards infinity. The problem is a result of the fact that, under these specific conditions, the set of Euler angles is not uniquely defined, as the first and third rotations are performed on the same physical direction.
To avoid these singularities, it becomes necessary to have two systems working on two different sets of Euler angles:

- one set of angles defined by three different indexes, which has the singularity condition on $\theta = (2n+1)\pi/2$;
- one set of angles where the first and the last indexes coincide, which has the singularity condition on $\theta = n\pi$.

To merge these two systems and avoid singularities, there are two main options:

- run both systems all the time, get the attitude kinematics only from one system until it reaches its singularity condition on θ, then switch to the other system, which will be further from its singularity;
- run just one system at a time; when the system reaches its singularity condition, convert from the current set of angles to the other set through the attitude matrix, impose the calculated angles as initial condition on the other system, then start the integration from where it was interrupted, deactivating the system that reached the singularity.

Although the first option is simpler, the second option offers significant computational savings for the simulation. It is important to note that the kinematics model is only executed in the simulation to calculate the satellite's motion over time and is not executed on the satellite processor. Despite the added complexity of the system switch, the second option was chosen to accelerate the execution of the Simulink model.

In the model discussed in this report, the 312 and 313 sets of Euler angles were chosen. The equations for the integration and the conversion to attitude matrix are reported below:

$$\begin{cases} \dot{\phi}_{312} = \dfrac{\omega_z \cos\psi - \omega_x \sin\psi}{\cos\theta} \\ \dot{\theta}_{312} = \omega_x \cos\psi + \omega_z \sin\psi \\ \dot{\psi}_{312} = \omega_y - (\omega_z \cos\psi - \omega_x \sin\psi)\tan\theta \end{cases} \qquad A_{312} = \begin{bmatrix} \cos\psi\cos\phi - \sin\psi\sin\phi\sin\theta & \cos\psi\sin\phi + \sin\psi\cos\phi\sin\theta & -\sin\psi\cos\theta \\ -\sin\phi\cos\theta & \cos\phi\cos\theta & \sin\theta \\ \sin\psi\cos\phi + \cos\psi\sin\phi\sin\theta & \sin\psi\sin\phi - \cos\psi\cos\phi\sin\theta & \cos\theta\cos\psi \end{bmatrix}$$

$$\begin{cases} \dot{\phi}_{313} = \dfrac{\omega_x \sin\psi + \omega_y \cos\psi}{\sin\theta} \\ \dot{\theta}_{313} = \omega_x \cos\psi - \omega_y \sin\psi \\ \dot{\psi}_{313} = \omega_z - \left(\omega_x \sin\psi + \omega_y \cos\psi\right)\cot\theta \end{cases} \qquad A_{313} = \begin{bmatrix} \cos\psi\cos\phi - \sin\psi\sin\phi\cos\theta & \cos\psi\sin\phi + \sin\psi\cos\phi\cos\theta & \sin\psi\sin\theta \\ -\sin\psi\cos\phi - \cos\psi\sin\phi\cos\theta & -\sin\psi\sin\phi + \cos\psi\cos\phi\cos\theta & \cos\psi\sin\theta \\ \sin\phi\sin\theta & -\cos\phi\sin\theta & \cos\theta \end{bmatrix}$$

In order to translate one set of Euler angles to the other set is sufficient to remember that A_{312} must be equal to A_{313}, since attitude matrices are both related to the same physical object. Inverting the formulas:

$$\begin{cases} \phi_{312} = \text{atan2}\left(-A^{2,1}, A^{2,2}\right) \\ \theta_{312} = \arcsin\left(A^{2,3}\right) \\ \psi_{312} = \text{atan2}\left(-A^{1,3}, A^{3,3}\right) \end{cases} \qquad \begin{cases} \phi_{313} = \text{atan2}\left(A^{3,1}, -A^{3,2}\right) \\ \theta_{313} = \arccos\left(A^{3,3}\right) \\ \psi_{313} = \text{atan2}\left(A^{1,3}, A^{2,3}\right) \end{cases} \tag{2}$$

The system switcher has been designed in Simulink using basic boolean operators. These operators are combined to generate a 'flag' signal that selects the appropriate system, taking into account the singularity conditions of both. In more detail, the switcher logic takes as input three boolean signals:

- $|\cos\theta_{312}| < tol$, where tol is a chosen tolerance value to keep the 312 system distant from the singularity;
- $|\sin\theta_{313}| < tol$, where tol is a chosen tolerance value to keep the 313 system distant from the singularity;
- the **flag** of the system at the previous step time.

A truth table can be created using the given signals and expected output. The truth table can then be simplified using basic logic operators such as AND, OR, and NOT through boolean algebra. Finally, the logic can be implemented in the simulation to handle the activation of the two systems.

6. Disturbances analysis

In order to make a realistic simulation of the rotating motion of the spacecraft, the environment distrubances has to be taken into account. The preliminary study of these external torques is crucial for a realistic simulation. In the following paragraphs a brief introduction will be done for all the main disturbances, then the simulation of the specific satellite and orbit will be presented, mainly to choose the two most relevant disturbances. This choice is reasonable since there are always two predominant effects of disturbance, while the other can be supposed small (usually some order of magnitude smaller, but always depends on the specific case).

6.1. Magnetic Disturbance

The influence of the Earth's magnetic field on the satellite is relevant due to the proximity of the orbit taken in exam. Besides the crucial role that it plays in the actuation, the magnetic field could also cause big disturbances on the satellite's dynamics. The magnetic torque, whether generated by the magnetorquers or by parasitic currents present in the satellite, follows the general law:

$$\boldsymbol{M} = \boldsymbol{D} \wedge \boldsymbol{B} \tag{3}$$

where $\boldsymbol{D}$ is the magnetic dipole generated by a coil or by parasitic currents, $\boldsymbol{B}$ is the magnetic field vector.
A mathematical model of the magnetic field is necessary to evaluate $\boldsymbol{B}$ given the satellite position along the orbit. The model chosen for the purpose is the 13th edition of the International Geomagnetic Reference Field (IGRF). According to this model, the magnetic field $\boldsymbol{B}$ is evaluated as the gradient of a magnetic scalar potential V, which is modelled as a spherical harmonic expansion of order N:

$$\boldsymbol{B}(r,\theta,\phi,t) = -\boldsymbol{\nabla} V(r,\theta,\phi,t) \qquad V(r,\theta,\phi,t) = a \sum_{n=1}^{N} \sum_{m=0}^{n} \left(\frac{a}{r}\right)^{n+1} \left(g^{n,m}(t)\cos m\phi + h^{n,m}(t)\sin m\phi\right) P^{n,m}(\cos\theta) \tag{4}$$

where r, θ, ϕ are the spherical coordinates of the satellite in a Earth-Centered Earth-Fixed (ECEF) frame, a is the Earth's equatorial radius (6371.2 km), $P^{n,m}(\cos\theta)$ are the Gauss normalized associated Legendre functions, $g^{n,m}(t)$

and $h^{n,m}(t)$ are the Schmidt semi-normalized spherical harmonic coefficients. These coefficients are computed from experimental data and depend on time, as the Earth magnetic field is not constant but changes significantly every year. In this simulation, the coefficients refer to year 2020 of IGRF-13 and the expansion is computed up to order 13. Note that the model must be in the ECEF frame because the magnetic field rotates with the Earth. To adapt the model to an Earth-Centered Inertial (ECI) frame, a rotation matrix is required for the input and its transpose for the output. The matrix takes account of the angular velocity of the planet on time. Lastly, the magnetic field $\boldsymbol{B}$ can be expressed in the body frame through the attitude matrix.
Once that $\boldsymbol{B}$ is defined for every satellite position, the $\boldsymbol{D}$ vector is chosen as an arbitrary constant (based on typical microsat values) and the torque is easily computed along the orbit thanks to the previous formula.

6.2. SRP Disturbance

SRP radiation torque is the disturbance generated by electromagnetic waves that impacts on the spacecraft panels and generate a force. These forces acting on some of the panels could give rise to a net torque around the center of mass of the spacecraft. Only sun radiation will be considered in this case, a more deep analysis should consider infrared Earth radiation and reflected Earth radiation. In addition, no eclipse condition will be analyzed during all the simulation, a reasonable assumption for the sun-synchronous case orbit.
The formula to calculate the force acting on each discrete panel is:

$$\boldsymbol{F_i} = -PA_i\left(\hat{S}_B \cdot \hat{N}_{B,i}\ \right)\left[(1-\rho_s)\hat{S}_B + \left(2\rho_s\left(\hat{S}_B \cdot \hat{N}_{B,i}\ \right) + \frac{2}{3}\rho_d\right)\hat{N}_{B,i}\right] \tag{5}$$

In order to simulate this kind of disturbance the coefficients of absorption, specular reflection and diffusion has to be decided. These values clearly depends on the material that will be choosen to construct the main body of the spacecraft, and the solar panels. Since these parameters are related through an energetic balance, we could only decide two of them and the third follows. In order to determine the force on each surface, also the geometry of the panels of the satellite has to be given, in particular size of each panel(fully defined in section ...) and direction of the normal of the panel in $\mathcal{B}$ frame. The direction of sun $\hat{S}_B$, has been firstly modeled in ECI frame considering the obliquity ϵ of earth's rotation axis with respect to the ecliptic plane, then through attitude matrix, the unit vector $\hat{S}_B$ has been computed. Lastly, to caluclate the torque we should known where the resulting force on each panel acts (i.e. the centre of SRP force for each panel). No detailed calulation has been made on this aspect, it is assumed as first approximation that the forces acts on the geometric center of the corresponding plate. Also, in order to correctly calculate the total torque a shadow check must be performed, this is simply implementated in Simulink by checkin the sign of the dot product of the normal versor of the plate and the sun direction.

6.3. Drag Disturbance

Over extended periods, the spacecraft's engagement with the higher strates of Earth's atmosphere results in the generation of a torque around its mass center. This influence may not be trivial. At altitudes less than 400 kilometers, the aerodynamic torque is the predominant factor, though its significance diminishes considerably beyond 700 kilometers altitude. For the simulation, the panels are considered from geometry data of section (..ref) the coefficient of drag C_d has been set to 2.2, the relative velocity consideres the rotation of Earth around its axis and also the rotation motion of the spacecraft. As for the SRP case, a sort of shadow check has to be implemented based on the dot product between the relative velocity and the normal of the surface. This check is required since the modelling of the surface is composed of two faces, usually one impacts with the relative air movement while the other is behind and doesn't impact. As for SRP disturbance, for the drag torque the vector r_i as distance of centre of pressure to centre of mass, should be evaluated. As a first approximation, the point of action of the force for each face is the middle point of the surface under consideration.

$$T_{AERO} = \begin{cases} \displaystyle\sum_{i=1}^{n} \vec{r_i} \times \vec{F_i} & \text{if } \vec{N}_{bi} \cdot \vec{v}^{b}_{rel} \geq 0 \\ 0 & \text{if } \vec{N}_{bi} \cdot \vec{v}^{b}_{rel} < 0 \end{cases} \qquad \text{with}$$
$$\vec{F_i} = -\frac{1}{2}\rho C_D v_{rel}^2 \vec{v}^{b}_{rel}(\vec{N}_{bi} \cdot \vec{v}^{b}_{rel})A_i \qquad \text{n=number of faces} \tag{6}$$

6.4. Gravity Gradient Disturbance

The gravity gradient disturbance account for the fact that the gravity around the spacecraft is not uniform, hence a non-negligible torque will arise from there. Studying the torque generated by an elementary force acting on the elementary mass dm the equation for this is obtained:

$$dM = -\mathbf{r} \times \frac{Gm_t dm}{|\mathbf{R}+\mathbf{r}|^3}(\mathbf{R}+\mathbf{r}) \tag{7}$$

Where **r** is the distance of dm from the centre of mass and **R** is the distance of the centre of mass from the centre of the Earth. Approximating this equation, and expressing the position vector of the centre of mass as the product of magnitude (R) with the direction cosines, it's possible to centre this torque in the principal inertia axes. Integrating this equation the final form is achieved.

$$\begin{aligned} M_x &= \frac{3Gm_t}{R^3}(I_z - I_y)c_2c_3 \\ M_y &= \frac{3Gm_t}{R^3}(I_x - I_z)c_1c_3 \\ M_z &= \frac{3Gm_t}{R^3}(I_y - I_x)c_1c_2 \end{aligned} \tag{8}$$

The c_1, c_2 and c_3 are the direction cosines of the radial direction in the principal axes. Therefore if one of the principal axes is aligned with the radial direction the torque will be zero because only one of the direction cosines is non-zero. It's clear that this disturbance acts in a continuous manner throughout the orbit motion and the torque produced depends mainly on the attitude matrix.
Instead, the stability configuration depends on the distribution of mass of the spacecraft with respect to the orientation we want to achieve. For our case of study, inspired by the ESAIL mission from ESA, the satellite is nadir pointing. In particular the $\boldsymbol{x_b}$ direction has to be aligned with the nadir, while the $\boldsymbol{z_b}$ has to point the sun for solar panels requirements. Using the numerical values of the spacecraft, and the orientation requriements just mentioned this particular configuration results unstable to GG disturbance.

6.5. Simulation of all disturbances

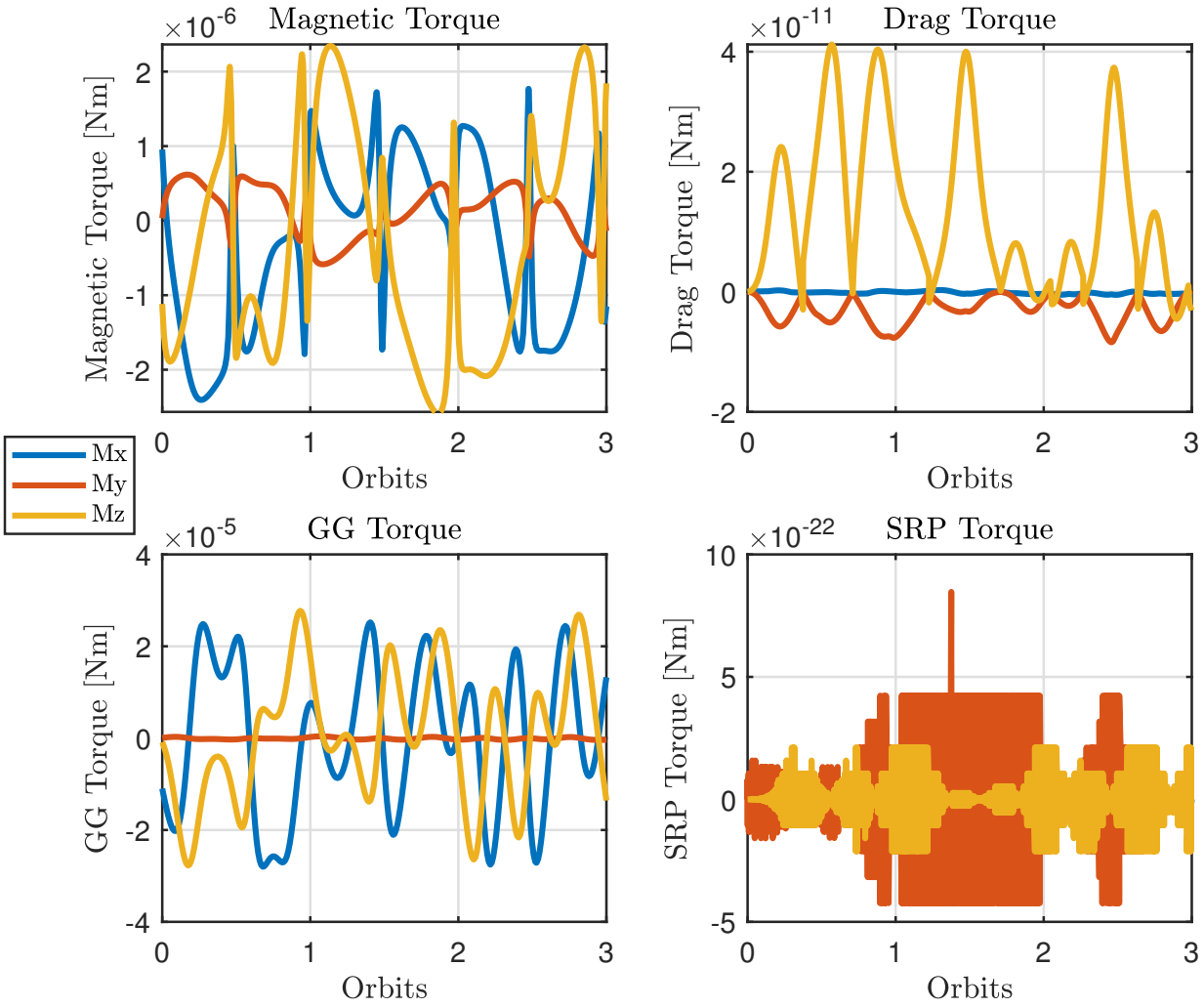

Figure 1: Simulation of all disturbances

The control-free motion has been simulated with all the disturbances for three full periods. The initial condition were set to null initial angular velocity and null Euler angles in the 312 set.
From the graphs of Figure 1 it is clear that SRP disturbance is negligible in our case, the graph shows only numerical zeros. In particular, this is due to the simmetry of the geometry of the spacecraft a small set off for the CoM would have produced a net torque. It is clear, that in this specific case, the two most relevant disturbances are due to magnetic field interaction and the gravity gradient torque since the atmospehric drag torque is some orders of magnitude smaller.
Note that in the Gravity Gradient torque the y-axis component is almost null compared to the other components along x and z, this is due to the fact that the y-axis component of the torque depends on the difference between inertia moment along x and along z, for our case those two moments of inertia are very similar (reference).

7. Sensors

Sensors are fundamental tools that allows the SC to know its orientation or angular velocity. Their presence onboard is fundamental for having a controlled motion of the satellite. In this section, the 3 sensors used will be presented, it will be also clarified the motivation that lead the team to choose two additional sensors over the horizon sensor assigned.

7.1. Horizon Sensor

Horizon sensors are devices that can detect the centre of the planet, in our case Earth, and reconstruct the direction of that point with respect to the satellite. They usually work by analyzing the IR spectrum of the image through a thermopile to reduce the visible light spectrum interference caused by transition of day and night on earth. Due to the nadir pointing requirment a static earth sensor has been chosen for this specific application. In particular, the *Meisei Earth Horizon* was chosen, which has the following specifics:

$F.O.V.$ [deg]	$Accuracy$ [deg]	$Frequency$ [Hz]
33	1	30

Table 1: Real data for Horizon Sensor

Due to operational requirements, the static sensor has to point the Earth, in particular the optical axis must have the same direction of the nadir (direction that links centre of earth and CoM of the S/C). To fulfill this request, a good option could be to position the sensor on the face that also contains the payload, that is the face of the spacecraft main body (cube) that has normal along the $\boldsymbol{x_b}$ direction. The model implemented to simulate the behaviour of the sensor in the Simulink environment, was to take the real position of the S/C with respect to centre of Earth expressed in inertial space, change its direction multiplying by -1 and express it in the $\mathcal{B}$ frame through the real attitude matrix $\boldsymbol{A_{B,N}}$. This unit vector is the input of the sensor block, here it is sampled through a zero-order hold of frequency specified by Table 1 to simulate the digital nature of the sensor. Then some errors of measurments has to be added. It was decided to model two typical effects of real sensor: the mounting error that cause misalignment and also an accuracy error modeled with a band-limited white noise on all the components of the direction vector.

7.2. Sun Sensor

Sun sensors are devices that detect the position of the Sun by measuring the incidence angle of its radiation on a sensor surface. This surface is typically made of materials that can generate a current proportional to the intensity of the incident light. From the measure of the current I generated by the sensor surface of area S, knowing the intensity of the radiation W and the coefficient α of the sensor, the angle of the incident light θ is internally computed as follows:

$$I = \alpha S W \cos\theta \implies \theta = \arccos\left(\frac{I}{\alpha S W}\right) \tag{9}$$

The unit vector pointing towards the Sun can be easily computed by the sensor using the knowledge of two angles obtained by placing two surfaces on different directions on the same plane.
As discussed in section 3, the satellite mission consists in pointing the Earth on a Sun-synchronous orbit with no eclipse periods. In view of this, it is important to prioritize accuracy over having the best Field of View (FOV) to select the sensor. For this reason, the choice falls upon a small and light Fine Sun sensor with good performances such as the *AAC Clyde Space SS200*:

F.O.V. **[deg]**	***Accuracy*** **[deg]**	***Frequency*** **[*Hz*]**
90	0.3	30

Table 2: Real data for Sun Sensor

This sensor has to be placed in the same direction as the solar panels, in the $\boldsymbol{z_b}$ direction, so the Sun is constantly visible (since the Orbit is Sun-synchronous). In order to not overcomplicate the Simulink model, it does not consider the FOV of the sensor, since in the detumbling manoeuvre the sensor is not used while in the tracking phase the Sun is always visible. To simulate the output of the real sensor, the model takes the Sun direction computed summing up the initial Earth-Sun vector with the position vector of the satellite in the inertial frame, which is computed through the keplerian dynamics. This vector is then normalized, reversed and brought in the body frame using the attitude matrix. From here, errors have been added in the same way as described for the horizon sensor (subsection 7.1).

Bibliography

[1] Georce C. Marshall Space Flight Center. *Saturn V Flight Manual SA-507*. National Aeronautics and Space Administration, 10 1969.